JBC RESEARCH ARTICLE

Cell-intrinsic Wnt4 ligand regulates mitochondrial oxidative phosphorylation in macrophages

Received for publication, May 9, 2022, and in revised form, June 9, 2022 Published, Papers in Press, June 25, 2022,
https://doi.org/10.1016/j.jbc.2022.102193

Mouna Tlili[1], **Hamlet Acevedo**[1], **Albert Descoteaux**[1], **Marc Germain**[2,3,4,‡], **and Krista M. Heinonen**[1,3,*,‡]

From the [1]*Institut national de recherche scientifique, Centre Armand Frappier Santé Biotechnologie, Laval, Canada;* [2]*Groupe de Recherche en Signalisation Cellulaire and Département de Biologie Médicale, Université du Québec à Trois-Rivières, Trois-Rivières, Canada;* [3]*Centre d'Excellence de Recherche sur les Maladies Orphelines – Fondation Courtois (CERMO-FC), Montreal, Canada;* [4]*Réseau Intersectoriel de Recherche en Santé de l'Université du Québec, Université du Québec, Quebec, Canada*

Edited by Ursula Jakob

Macrophages respond to their environment by adopting a predominantly inflammatory or anti-inflammatory profile, depending on the context. The polarization of the subsequent response is regulated by a combination of intrinsic and extrinsic signals and is associated with alterations in macrophage metabolism. Although macrophages are important producers of Wnt ligands, the role of Wnt signaling in regulating metabolic changes associated with macrophage polarization remains unclear. Wnt4 upregulation has been shown to be associated with tissue repair and suppression of age-associated inflammation, which led us to generate Wnt4-deficient bone marrow–derived macrophages to investigate its role in metabolism. We show that loss of Wnt4 led to modified mitochondrial structure, enhanced oxidative phosphorylation, and depleted intracellular lipid reserves, as the cells depended on fatty acid oxidation to fuel their mitochondria. Further we found that enhanced lipolysis was dependent on protein kinase C–mediated activation of lysosomal acid lipase in Wnt4-deficient bone marrow–derived macrophages. Although not irreversible, these metabolic changes promoted parasite survival during infection with *Leishmania donovani*. In conclusion, our results indicate that enhanced macrophage fatty acid oxidation impairs the control of intracellular pathogens, such as *Leishmania*. We further suggest that Wnt4 may represent a potential target in atherosclerosis, which is characterized by lipid storage in macrophages leading to them becoming foam cells.

Macrophages possess multiple functions, ranging from pathogen clearance and antigen presentation to T lymphocytes to tissue remodeling and immune suppression (1–3). By analogy with the cytokine responses generated, macrophages have been long divided into two main categories: classically activated proinflammatory macrophages (M1) and alternatively activated anti-inflammatory macrophages (M2) (4–7). These two differentiation profiles have also been characterized by their diverging cellular metabolism (8–10). M1 macrophages upregulate glycolytic enzymes and preferentially use glucose as their main energy source, resulting in ATP production through the conversion of pyruvate to lactate (9, 11). In contrast, M2 macrophage metabolism is supported by high mitochondrial activity and oxidative phosphorylation (OXPHOS), fueled at least in part by fatty acid oxidation (FAO) (12, 13).

Macrophage polarization is regulated by a combination of intrinsic and extrinsic signals, such as cytokines, growth factors, and microbial products. Wnt signaling is known for its pleiotropic effects in cell fate decisions during development and tissue repair, but although macrophages are known to express several Wnt ligands, the role of individual Wnt proteins in macrophage polarization is not well established (14). The prototypical canonical ligand that promotes β-catenin translocation into the nucleus, Wnt3a, increases arginase expression in primary macrophages after bacterial infection and inhibits the secretion of proinflammatory cytokines (15, 16). Conversely, Wnt5a, which is usually associated with β-catenin–independent noncanonical Wnt signaling, promotes inflammatory responses *via* the transcription factor NF-κB to ensure immune surveillance (17), and both Wnt5a and NF-κB expression are increased upon macrophage exposure to mycobacteria (16). However, the role of Wnt signaling in macrophage metabolism has not been investigated in depth.

We have focused our study on Wnt4, a mostly noncanonical ligand (18, 19), whose expression is upregulated in lung macrophages upon injury to promote tissue repair (20). Wnt4 overexpression in bone marrow was shown to inhibit age-associated inflammation (21), while its deletion from dendritic cells impacts their differentiation and promotes the development of type 2 immunity in response to the hookworm parasite *Nippostrongylus brasiliensis* (19). We thus hypothesized that Wnt4 could also contribute to the metabolic reprogramming of bone marrow–derived macrophages (BMDMs).

We show that Wnt4-deficient BMDMs display reduced AKT (Thr308) and ERK1/2 phosphorylation but increased ATP levels, which can be attributed to an enhanced mitochondrial OXPHOS activity. Furthermore, we identify FAO as a principal mechanism involved in the increase in mitochondrial activity. However, while Wnt4-deficient macrophages respond more

‡ These authors contributed equally to this work.
* For correspondence: Krista M. Heinonen, krista.heinonen@inrs.ca.

strongly to lipopolysaccharide (LPS)/M1-type stimulation, their altered FA metabolism favors replication of the protozoan parasite *Leishmania donovani*. Wnt4-mediated regulation of macrophage metabolism and mitochondrial activity thus appear important for the control of intracellular pathogens.

Results

Wnt4 promotes AKT (Thr308) and ERK signaling

To elucidate the importance of *Wnt4* in macrophages, we generated conditional knock-out mice in which *Wnt4* is deleted from most macrophages and granulocytes by LysM-Cre–mediated excision ($Wnt4^{\Delta/\Delta}$ mice) (22, 23). These mice present no overt alterations in myeloid differentiation *in vivo* (24). We isolated BM cells from $Wnt4^{\Delta/\Delta}$ and Cre$^-$ littermate control mice, and we obtained comparable numbers of $Wnt4^{\Delta/\Delta}$ and control BMDM after 1 week in culture (Fig. 1, *A* and *B*). While *Wnt4* deletion was highly efficient in culture (Fig. 1*C*), $Wnt4^{\Delta/\Delta}$ and control BMDM expressed similar levels of the macrophage surface marker F4/80 (Fig. 1*D*), suggesting that Wnt4 deficiency did not significantly alter BMDM differentiation from BM progenitors. There was no difference in β-catenin phosphorylation (Fig. 1*E*) or in the activation of c-Jun N-terminal protein kinase (JNK) (Fig. 1, *F* and *G*), suggesting that the deletion of Wnt4 did not alter the balance between canonical and JNK-dependent noncanonical signaling in the absence of other exogenous ligands.

Macrophage function is regulated not only by JNK but also other members of the mitogen-activated protein kinase (MAPK) family, such as the extracellular signal–regulated kinases 1 and 2 (ERK1/2) (25, 26). Unlike JNK, there was a notable decrease in ERK1/2 phosphorylation in $Wnt4^{\Delta/\Delta}$ BMDM (Fig. 1,*H* and *I*). $Wnt4^{\Delta/\Delta}$ BMDM also showed a decreased level of AKT phosphorylation on Thr308 (Fig. 1, *J* and *K*), suggesting that these signal transduction pathways

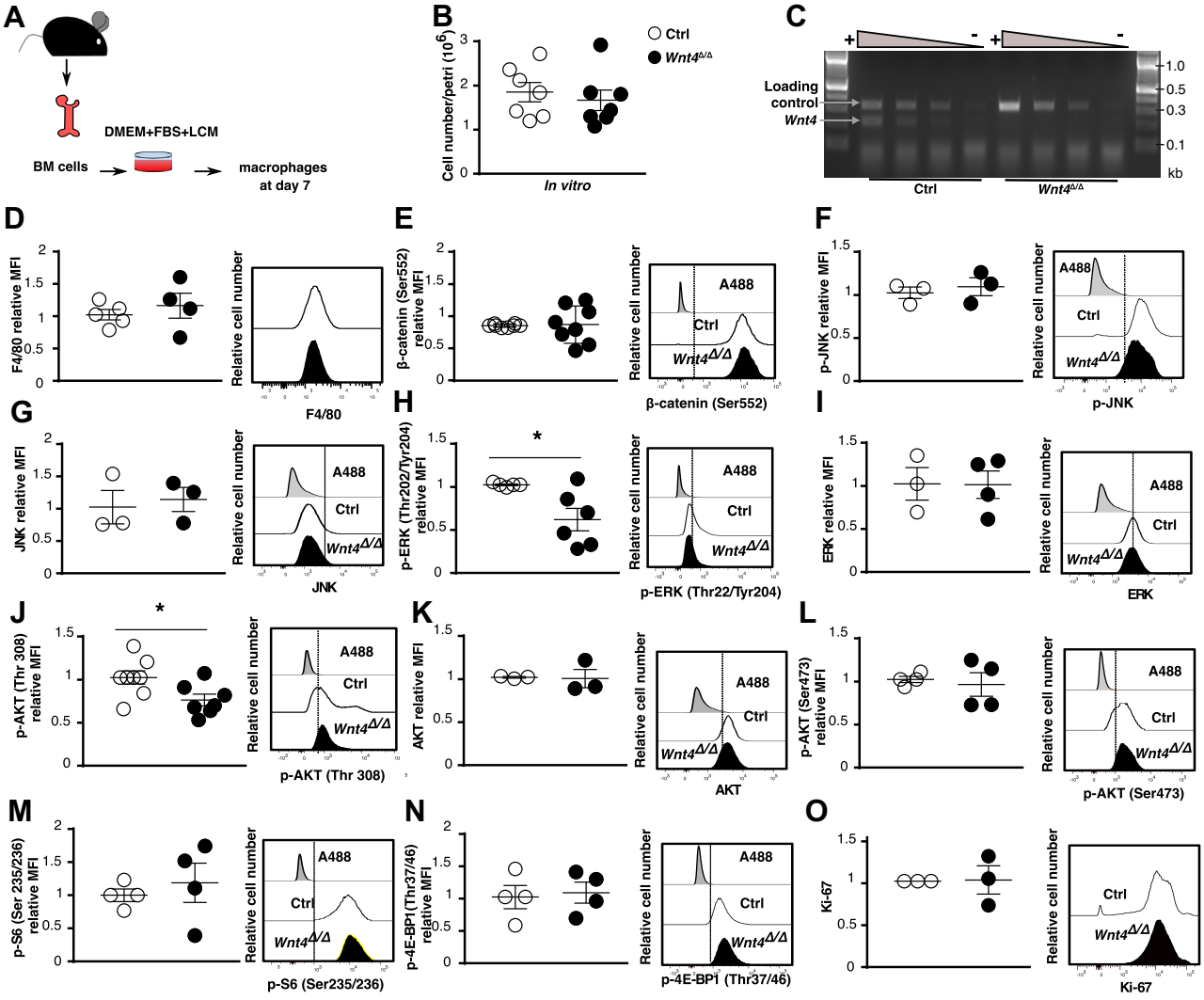

Figure 1. Endogenous Wnt4 promotes AKT (Thr308) and ERK1/2 phosphorylation in macrophages. *A*, bone marrow–derived macrophage (BMDM) differentiation. *B*, number of macrophages collected after 7 days of differentiation in culture. *C*, PCR analysis of decreased DNA concentration extracted from mouse tail sample. *D–O*, relative mean fluorescence intensity (MFI) of F4/80 (*D*), phospho-β-catenin (Ser522) (*E*), phospho-JNK (Thr183/Tyr185) (*F*), JNK (*G*), phospho-ERK1/2 (Thr202/Tyr204) (*H*), ERK1/2 (*I*), phospho-AKT (Thr308) (*J*), AKT (*K*), phospho-AKT (Ser473) (*L*), phospho-S6 (Ser235/Ser236) (*M*), phospho-4EBP-1 (Thr37/Thr46) (*N*), and Ki-67 (*O*) in unstimulated BMDM. The histograms represent compiled data from three to eight animals per group (mean + SEM). *$p < 0.05$ (two-tailed, paired Student's *t* test).

are altered in these cells. Nevertheless, phosphorylation of the mTORC2-dependent site in AKT (Ser473) (Fig. 1*L*), as well as that of the mTORC1 downstream effectors S6 (Ser235/236) (Fig. 1*M*) and 4EBP1(Thr37/46) (Fig. 1*N*) was not affected in *Wnt4*$^{\Delta/\Delta}$ BMDM, indicating that Wnt4 regulates ERK1/2 and AKT signaling independently from the mTORC axis.

Considering the dual roles of ERK1/2 and AKT in cell proliferation and metabolism (27–29), we further evaluated the proliferative state of *Wnt4*$^{\Delta/\Delta}$ BMDM using Ki-67. Ki-67 expression was not significantly changed in *Wnt4*$^{\Delta/\Delta}$ BMDM compared to control (Fig. 1*O*), which together with the comparable cell counts (Fig. 1*B*) suggests that Wnt4 does not affect BMDM proliferation. However, impaired ERK1/2 and AKT (Thr308) activation prompted us to further investigate the functional consequences of Wnt4 deletion on BMDM metabolism.

Wnt4 deficiency increases ATP production through OXPHOS

To address the impact of Wnt4 on macrophage metabolism, we first investigated their ATP levels. *Wnt4*$^{\Delta/\Delta}$ BMDM displayed higher intracellular ATP levels (Fig. 2*A*) but a comparable ADP/ATP ratio relative to control cells (Fig. 2*B*), suggesting that this increase in ATP is not the consequence of alterations in ATP consumption. In addition, intracellular ATP was decreased to similar levels in both genotypes upon inhibition of the ATP synthase with oligomycin (Fig. 2*A*). As these

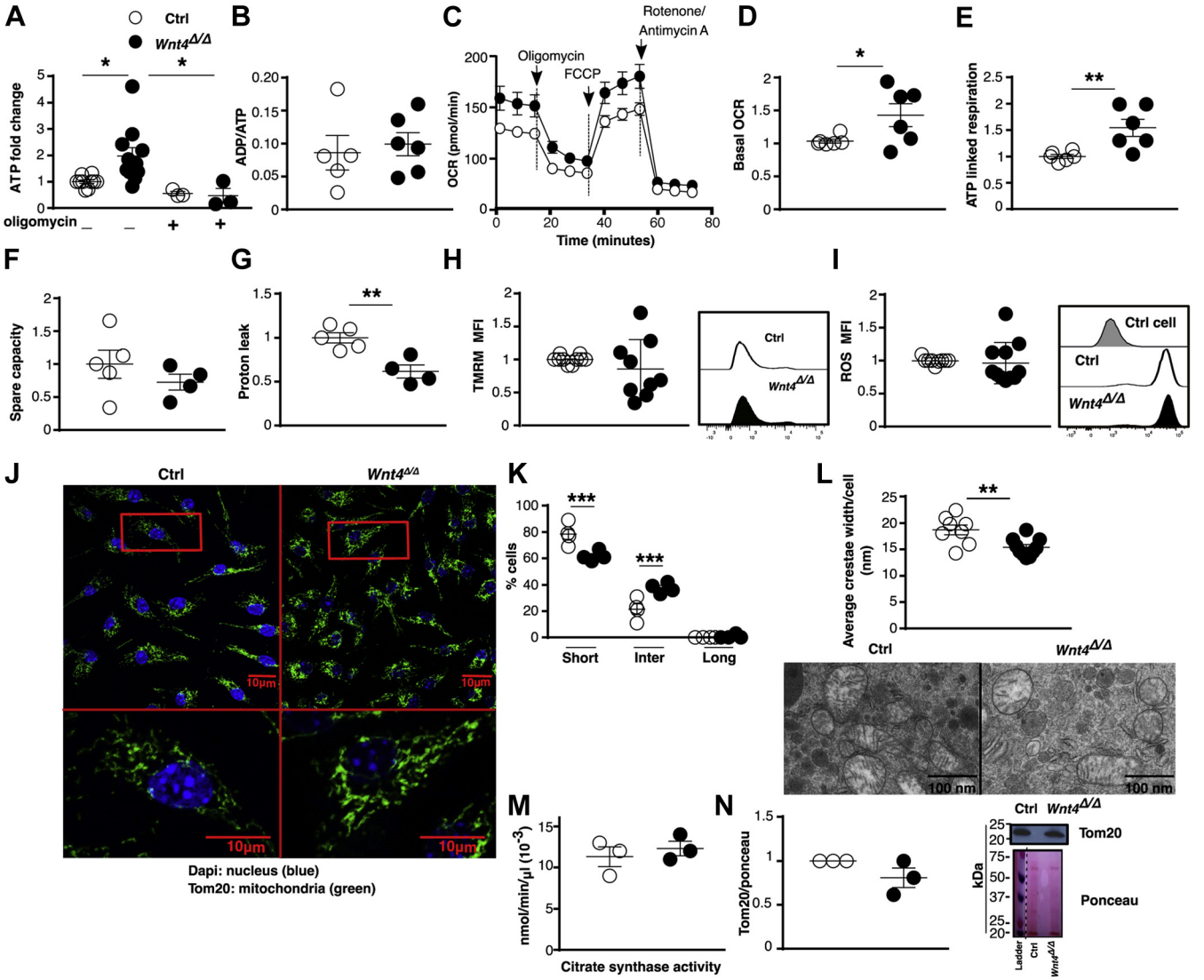

Figure 2. Wnt4 deletion increases mitochondrial energy metabolism. *A*, intracellular ATP oligomycin. *B*, ATP/ADP ratio. *C*, representative oxygen consumption rate (OCR) curves. *D*, basal OCR normalized to control. *E*, ATP linked-respiration (OCR after oligomycin injection—basal OCR). *F*, spare respiratory capacity (OCR after FCCP injection—basal OCR). *G*, proton leak (OCR after oligomycin injection—OCR after rotenone/antimycin A injection). *H*, measure of mitochondrial membrane potential as determined by relative TMRM MFI. *I*, mitochondrial ROS production as measured by relative Mitosox MFI. *J*, confocal microscopy images of BMDM staining for mitochondria (green: TOM20, blue: nucleus, 60×). *K*, analysis of mitochondrial length, represented as proportion of BMDM with predominantly short, intermediate, or long mitochondria. *L*, mitochondrial cristae width, represented as average width/cell from 10 individual cells per condition as measured from electron microscopy images. Representative transmission electron microscopy images are shown below (20,000). *M*, intracellular citrate synthase activity. *N*, quantification and representative immunoblot for TOM20. The histograms represent compiled data from three to six animals per group (mean + SEM). *$p < 0.05$, **$p < 0.01$, ***$p < 0.001$ (two-tailed, unpaired Student's *t* test (for two groups) or one-way ANOVA multiple comparisons). MFI, mean fluorescence intensity; TMRM, tetramethylrhodamine methyl ester; BMDM, bone marrow–derived macrophage.

data suggest that OXPHOS is increased in *Wnt4*$^{\Delta/\Delta}$ BMDM, we measured oxygen consumption rates (OCRs) in control and *Wnt4*$^{\Delta/\Delta}$ BMDM. Consistent with *Wnt4*$^{\Delta/\Delta}$ BMDM having increased OXPHOS activity, basal OCR was significantly increased in these cells (Fig. 2, *C* and *D*). ATP-linked respiration was also increased in *Wnt4*$^{\Delta/\Delta}$ BMDM (Fig. 2*E*), further supporting a role for OXPHOS in the elevated cellular ATP levels observed in *Wnt4*$^{\Delta/\Delta}$ cells. On the other hand, the spare respiratory capacity (a measure of the ability of mitochondria to respond to an increased energy demand) (Fig. 2*F*) was similar between the two genotypes while proton leak (a measure of proton diffusion across the inner membrane) (Fig. 2*G*) was decreased in *Wnt4*$^{\Delta/\Delta}$ BMDM. In addition, mitochondrial membrane potential and mitochondrial ROS levels in *Wnt4*$^{\Delta/\Delta}$ BMDM were comparable to controls (Fig. 2,*H* and *I*). Altogether, our results indicate that mitochondria in *Wnt4*$^{\Delta/\Delta}$ cells have increased flux through the electron transport chain and ATP synthase without major impairment in mitochondrial function.

We then determined if the functional changes we observed in *Wnt4*$^{\Delta/\Delta}$ BMDM were associated with changes in mitochondrial structure or mass. We first stained mitochondria in control and *Wnt4*$^{\Delta/\Delta}$ BMDM macrophages for the mitochondrial outer membrane protein TOM20 and imaged them by confocal microscopy (Fig. 2*J*). While control BMDM had on average very short mitochondria, we observed a significant increase in intermediate mitochondria in *Wnt4*$^{\Delta/\Delta}$ BMDM (Fig. 2*K*). Mitochondrial elongation and increased OXPHOS can be associated with changes in cristae structure, the folds of the inner membrane where the electron transport chain resides. We thus used electron microscopy to evaluate cristae width in control and *Wnt4*$^{\Delta/\Delta}$ BMDM. *Wnt4*$^{\Delta/\Delta}$ BMDM had tighter cristae than their control counterparts (Fig. 2*L*), suggesting improved OXPHOS efficiency. On the other hand, there was no difference in mitochondrial mass as measured by citrate synthase activity (Fig. 2*M*) or TOM20 immunoblotting (Fig. 2*N*). In sum, these findings indicate that Wnt4 controls mitochondrial activity without altering mitochondrial mass.

Lipolysis is enhanced in Wnt4$^{\Delta/\Delta}$ *macrophages*

As our results suggest that the increased OCR and ATP levels observed in *Wnt4*$^{\Delta/\Delta}$ BMDM is the consequence of increased metabolic flow through OXPHOS rather than a major change in mitochondrial structure, we then analyzed the potential substrates supporting OXPHOS in these cells. *Wnt4*$^{\Delta/\Delta}$ BMDM showed a substantial decrease in lactate production (Fig. 3*A*), which was associated with a smaller but significant reduction in glucose consumption (Fig. 3*B*). While these results are consistent with the greater OXPHOS activity, we observed they also suggest that glucose is not the major source of metabolic intermediates supporting enhanced mitochondrial activity in *Wnt4*$^{\Delta/\Delta}$ BMDM. In contrast, there was a drastic reduction in the lipid droplets present in *Wnt4*$^{\Delta/\Delta}$ BMDM relative to control cells, as measured by Oil Red O staining (Fig. 3, *C* and *D*), suggesting that fatty acids (FAs) could be fueling the increased OXPHOS in these cells.

Lipid droplets store triglycerides that must be hydrolyzed to liberate the FA used in mitochondrial ß-oxidation. As lysosomal acid lipase (LAL) is one of the key enzymes that cells use to liberate FA from lipid droplets (30, 31), we measured its activity in control and *Wnt4*$^{\Delta/\Delta}$ BMDM. Consistent with the reduction in lipid droplets, LAL activity was increased 2-fold in *Wnt4*$^{\Delta/\Delta}$ BMDM as compared to controls (Fig. 4*A*). However, this increase is neither due to an increase in *Lipa* gene expression (Fig. S1*A*) nor to an increase in the overall lysosomal content as we did not observe any change in the activity of the lysosomal protease Cathepsin B (Fig. 4*B*) or the expression of the lysosomal membrane protein LAMP-1 (Fig. 4*C*). Moreover, LAL inhibition restored cytosolic lipid content in *Wnt4*$^{\Delta/\Delta}$ BMDM (Fig. 4, *D* and *E*). Consistent with a specific role for LAL, the cytosolic neutral lipase activity was similar between *Wnt4*$^{\Delta/\Delta}$ and control BMDM (Fig. 4*F*), and the genes for the enzymes responsible for this activity, *Lipe* and *Pnpla2*, were expressed at very low levels but similar levels in both genotypes (Fig. S1, *B* and *C*). Altogether these data indicate that enhanced LAL activity is responsible of FA generation in *Wnt4*$^{\Delta/\Delta}$ cells.

As autophagy has been implicated in LAL-dependent lipid metabolism in macrophages (32), we assessed autophagy flux with the membrane autophagosome marker LC3. Although we observed a decrease in the number of LC3 puncta in *Wnt4*$^{\Delta/\Delta}$ BMDM that was partially rescued with bafilomycin treatment (Fig. 4,*G* and *I*), there was no significant increase in the ratio of LC3 puncta (treated/untreated) between *Wnt4*$^{\Delta/\Delta}$ BMDM and controls (Fig. 4*H*), indicating that the autophagic flux was not enhanced in *Wnt4*$^{\Delta/\Delta}$ BMDM. Put together, these data point toward increased lipid degradation by LAL in *Wnt4*$^{\Delta/\Delta}$ BMDM, irrespective of alterations in autophagy.

Wnt4$^{\Delta/\Delta}$ *BMDM shows increased mitochondrial β-oxidation*

Decreased glucose consumption and decreased lipid storage support the hypothesis of FAO as a major source of energy in *Wnt4*$^{\Delta/\Delta}$ BMDM. To more directly evaluate the relative importance of each carbon source, we inhibited glycolysis with 2-deoxy-d-glucose (2-DG) or FA transport into mitochondria using etomoxir. We then measured OCR in otherwise unstimulated and nonpolarized macrophages, similar to Figure 2. Control BMDM showed very little alteration in their basal OCR in response to blocking either one of the two pathways (Fig. 5, *A*–*C*), likely reflecting their relatively low level of metabolic activity in the absence of stimulation (33). Consistent with ß-oxidation providing the extra carbon source to fuel OXPHOS in *Wnt4*$^{\Delta/\Delta}$ cells, etomoxir significantly decreased basal OXPHOS in these cells. Similarly, etomoxir significantly reduced ATP-linked OCR in *Wnt4*$^{\Delta/\Delta}$ but not in control BMDM (Fig. 5*D*), and it also increased the spare capacity of *Wnt4*$^{\Delta/\Delta}$ BMDM but not of control cells (Fig. 5*E*). Moreover, *Wnt4*$^{\Delta/\Delta}$ BMDM challenged with palmitate showed a significant decrease in OCR upon etomoxir treatment while control BMDM was not affected (Fig. 5*F*). This coincided with an increase in Oil Red O staining in etomoxir-treated *Wnt4*$^{\Delta/\Delta}$ BMDM, restoring their lipid droplets to control levels (Fig. 5,

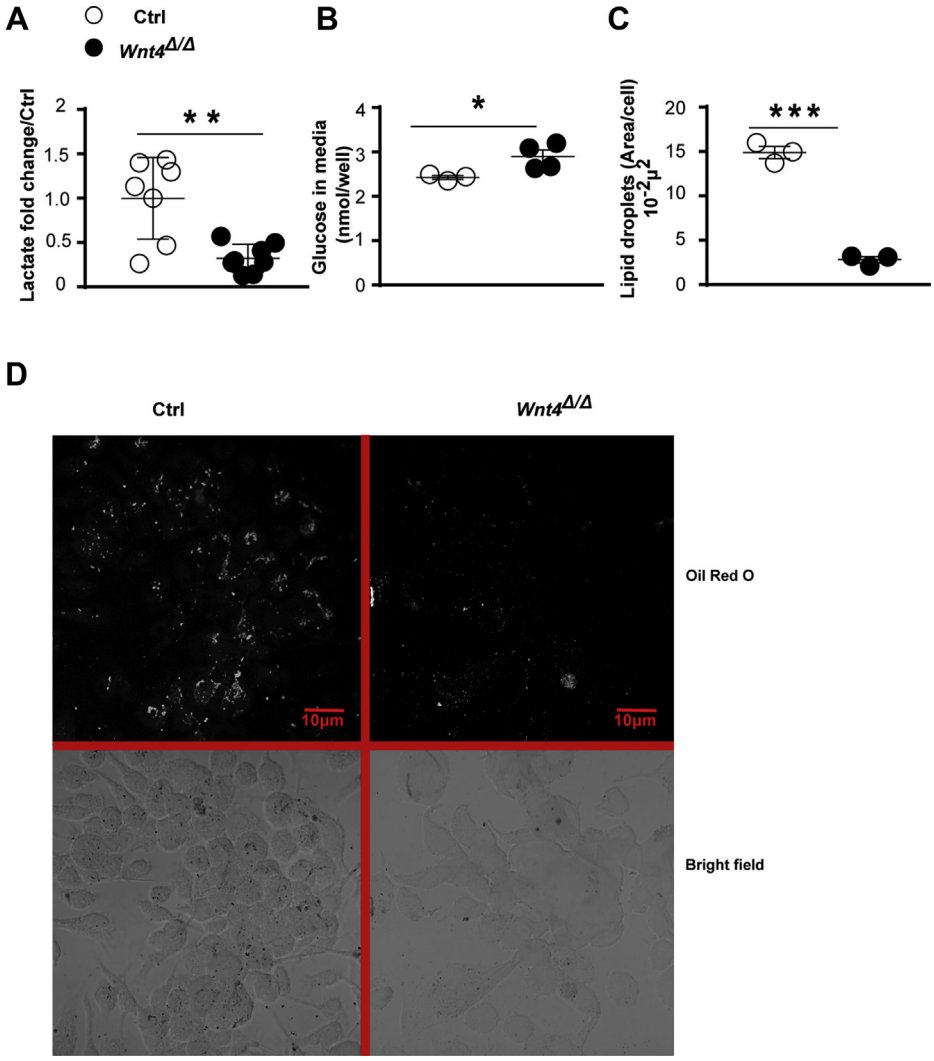

Figure 3. Wnt4 deletion decreases glycolysis and intracellular lipid storage. *A*, total lactate (intracellular + extracellular). *B*, glucose remaining in culture media. *C*, quantification of lipid droplets as determined by the area of Oil Red O staining per cell quantified using ImageJ. *D*, representative confocal microscopy images showing Oil Red O signal in BMDM (60X). The histograms represent compiled data from three to eight animals per group (mean + SEM). $^{*}p < 0.05$, $^{**}p < 0.01$, $^{***}p < 0.001$ (two-tailed, unpaired Student's *t* test). BMDM, bone marrow–derived macrophage.

G and *H*) and further supports a role for ß-oxidation in the metabolic changes observed in $Wnt4^{\Delta/\Delta}$ BMDM. Treatment with 2-DG also somewhat decreased basal OCR in $Wnt4^{\Delta/\Delta}$ BMDM (Fig. 5, *A*–*C*), suggesting that glucose can also contribute to their enhanced OXPHOS. However, the expression of *Pdh1*, an enzyme required to commit pyruvate to the TCA cycle, was not enhanced in $Wnt4^{\Delta/\Delta}$ BMDM (Fig. S1*D*), suggesting no major changes in pyruvate handling by $Wnt4^{\Delta/\Delta}$ BMDM. Altogether, these results indicate that the loss of Wnt4 stimulates the usage of lipids as an important source of energy.

To better establish how Wnt4 regulates lipid metabolism, we evaluated putative signaling pathways downstream of Wnt4. While JNK phosphorylation (Fig. 1, *E* and *F*) and AKT-dependent β-catenin phosphorylation were not altered in $Wnt4^{\Delta/\Delta}$ BMDM (Fig. 1*D*), the classical β-catenin-dependent target genes *c-Myc* and *Ccnd1* (*Axin2* was not expressed in BMDM) were downregulated in $Wnt4^{\Delta/\Delta}$ BMDM (Fig. S1, *E* and *G*). As the noncanonical protein kinase C (PKC)/Ca^{2+} pathway negatively regulates TCF/β-catenin-dependent gene expression without impacting intracellular β-catenin levels (34) and inhibits ERK1/2 (35), our results suggest that the absence of Wnt4 promotes the activation of this PKC pathway. Since PKC activity has also been associated with LAL induction during monocyte differentiation into macrophage (36), we evaluated the impact of PKC inhibition on LAL activity in $Wnt4^{\Delta/\Delta}$ BMDM. While PKC inhibition had no impact on control BMDMs, LAL activity in $Wnt4^{\Delta/\Delta}$ BMDM was reduced to control levels upon PKC inhibition (Fig. 5*I*), suggesting that the enhanced lipolysis observed in the absence of Wnt4 is PKC-dependent. Considering the decrease in AKT (Thr308) phosphorylation observed in $Wnt4^{\Delta/\Delta}$ BMDM (Fig. 1*I*), we also evaluated the contribution of the PI3K/PTEN axis. To our surprise, LAL activity was further enhanced in $Wnt4^{\Delta/\Delta}$ BMDM upon PTEN inhibition (Fig. 5*J*). While we cannot exclude a potential contribution of AKT downstream of PI3K upon PTEN inhibition, it is possible that the increase in PI3K activity triggered by PTEN inhibition promotes PKC activation

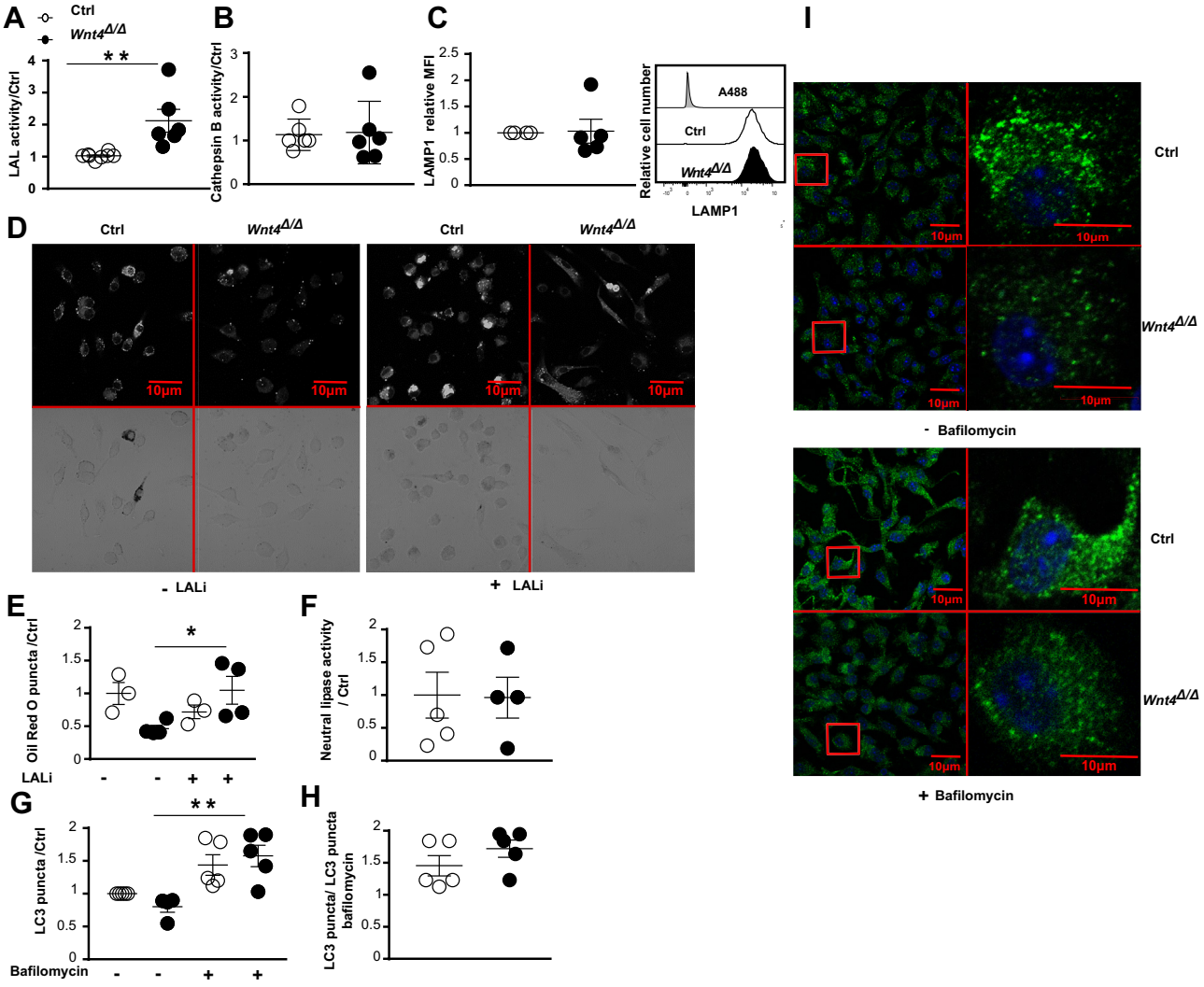

Figure 4. LAL promotes fatty acid usage in *Wnt4*$^{\Delta/\Delta}$ BMDM. *A*, lysosomal acid lipase (LAL) activity, normalized to controls. *B*, cathepsin B activity, normalized to controls. *C*, quantification of lysosomes as determined by relative LAMP-1 MFI. *D*, representative confocal microscopy images showing Oil Red O signal in BMDM in the absence and the presence of a LAL inhibitor (LALi)(60×). *E*, quantification of lipid droplets as determined by the area of Oil Red O staining per cell quantified using ImageJ. *F*, neutral lipase activity, normalized to controls. *G*, quantification of LC3 puncta per cell ± bafilomycin (100 nmol) with ImageJ software. *H*, quantification of the LC3puncta/LC3 puncta + bafilomycin ratio to evaluate autophagy flux. *I*, representative confocal microscopy images of BMDM, staining for autophagosomes (*green*: LC3, *blue*: nucleus, 60×). *$p < 0.05$, **$p < 0.01$ (two-tailed, unpaired Student's *t* test (two groups) or one-way ANOVA multiple comparisons). BMDM, bone marrow–derived macrophage; MFI, mean fluorescence intensity.

via PDK-1 (37, 38). In sum, these results strongly suggest that PKC and PI3K signaling regulate lipolysis in *Wnt4*$^{\Delta/\Delta}$ BMDM.

Wnt4 is not required for the inflammatory response induced by LPS stimulation

Thus far, we have established that *Wnt4*$^{\Delta/\Delta}$ BMDMs have higher ATP levels, mostly as a consequence of increased mitochondrial FAO, which has been generally associated with macrophage polarization to an M2 profile (30, 39). However, flow cytometry analysis revealed no significant differences in the expression of M1 (CD86, MHCII) or M2 cell surface markers (CD206) between unstimulated *Wnt4*$^{\Delta/\Delta}$ and control BMDM (Fig. 6, *A*–*C*). There was also no difference in cathepsin B activity (Fig. 4*B*), the most abundant lysosomal protease (40) whose activity has been shown to be increased in M2 macrophages (41). In summary, the metabolic differences in *Wnt4*$^{\Delta/\Delta}$ BMDM did not appear to result in an inherent bias in unstimulated cells.

LPS is a toll-like receptor 4 agonist that is widely used to promote the secretion of proinflammatory cytokines by macrophages (42). Moreover, LPS-treated macrophages reduce their oxygen consumption and adopt a strongly glycolytic profile (10). We thus stimulated *Wnt4*$^{\Delta/\Delta}$ and control BMDM with LPS to determine if the metabolic differences in *Wnt4*$^{\Delta/\Delta}$ BMDM were reversible. There was a strong suppression of OCR in LPS-treated *Wnt4*$^{\Delta/\Delta}$ BMDM, with basal OCR decreasing even slightly below levels detected in LPS-treated controls (Fig. 6, *D* and *E*). Unsurprisingly, this also corresponded to a significant decrease in ATP-linked respiration (Fig. 6*F*), indicating that LPS inhibits mitochondrial activity in both *Wnt4*$^{\Delta/\Delta}$ and control BMDM. Similarly, extracellular acidification rate was increased to similar levels in LPS-treated *Wnt4*$^{\Delta/\Delta}$ and control BMDM, suggesting an increase in lactate

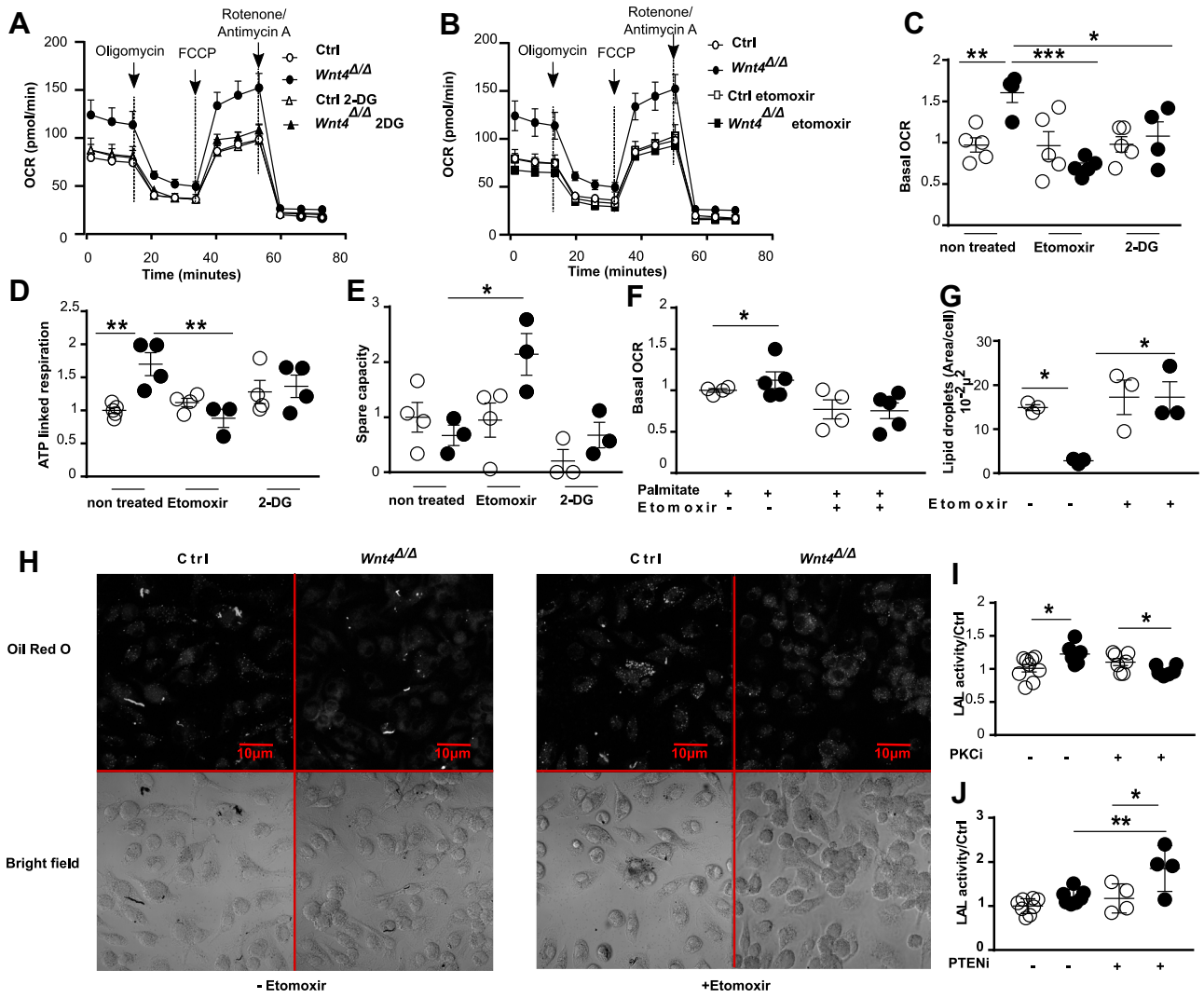

Figure 5. Wnt4 deletion enhances β-oxidation. *A* and *B*, representative oxygen consumption rate (OCR) curves for BMDM pretreated or not with 2-DG (5 mM) (*A*) to block glycolysis or etomoxir (250 μM) (*B*) to block β-oxidation. *C–E*, quantification of basal OCR (*C*), ATP-linked respiration (*D*), and spare respiratory capacity (*E*) with and without 2-DG or etomoxir. *F*, quantification of basal OCR in BMDM exposed to palmitate in the absence or the presence of etomoxir. *G*, quantification of Oil Red O positive area per cell ± etomoxir. *H*, representative confocal microscopy images of Oil Red O signal in BMDM ± etomoxir (60×). *I–J*, lysosomal acid lipase (LAL) activity in BMDM treated with a PKC inhibitor (5 μM) (*I*) or a PTEN inhibitor (100 nM) (*J*), normalized to controls. The histograms represent compiled data from six animals per group (mean ± SEM). $*p < 0.05$, $**p < 0.01$, $***p < 0.001$ (ordinary one-way ANOVA, multiple comparisons). 2-DG, 2-deoxy-d-glucose; BMDM, bone marrow–derived macrophage; PKC, protein kinase C.

production (Fig. 6*G*). These data indicate that the LPS-induced metabolic switch to glycolysis is not impaired in *Wnt4*$^{Δ/Δ}$ BMDM.

To further evaluate the inflammatory potential of *Wnt4*$^{Δ/Δ}$ BMDM, we measured nitric oxide (NO) and TNFα production in culture supernatants with and without LPS stimulation. *Wnt4*$^{Δ/Δ}$ BMDM produced slightly more NO (Fig. 6*H*) and similar levels of TNFα (Fig. 6*I*) upon LPS stimulation as compared to their normal counterparts. Furthermore, *Wnt4*$^{Δ/Δ}$ and control BMDM showed a comparable expression of M1 (iNOS) and M2 (arginase-1) markers following LPS/IFN-γ and IL-4/IL-13/IL-10-mediated polarization, respectively (Fig. S1, *H* and *I*). These data confirm that the capacity of *Wnt4*$^{Δ/Δ}$ BMDM to respond to a strong proinflammatory stimulus was not negatively affected by the metabolic alterations seen at steady state.

Wnt4 deficiency contributes to the ability of L. donovani promastigotes to colonize BMDM

Metabolic alterations in *Wnt4*$^{Δ/Δ}$ BMDM did not prevent their polarization or LPS-induced glycolytic switch. If anything, the response of *Wnt4*$^{Δ/Δ}$ BMDM was even stronger than controls (Fig. 6, *E* and *H*). To evaluate if *Wnt4*$^{Δ/Δ}$ BMDM was predisposed to respond more strongly to other stimuli, we investigated their response in a more physiologically relevant context, following a parasitic infection.

Macrophages are the principal hosts of the intracellular parasite *Leishmania* and are indispensable for their survival and replication (43). Importantly, macrophage polarization toward an M2 profile promotes parasite growth (44, 45). Here, we compared the fate of *L. donovani* metacyclic promastigotes in wildtype and *Wnt4*$^{Δ/Δ}$ BMDM. There was no significant difference in parasite uptake 6h postinfection between

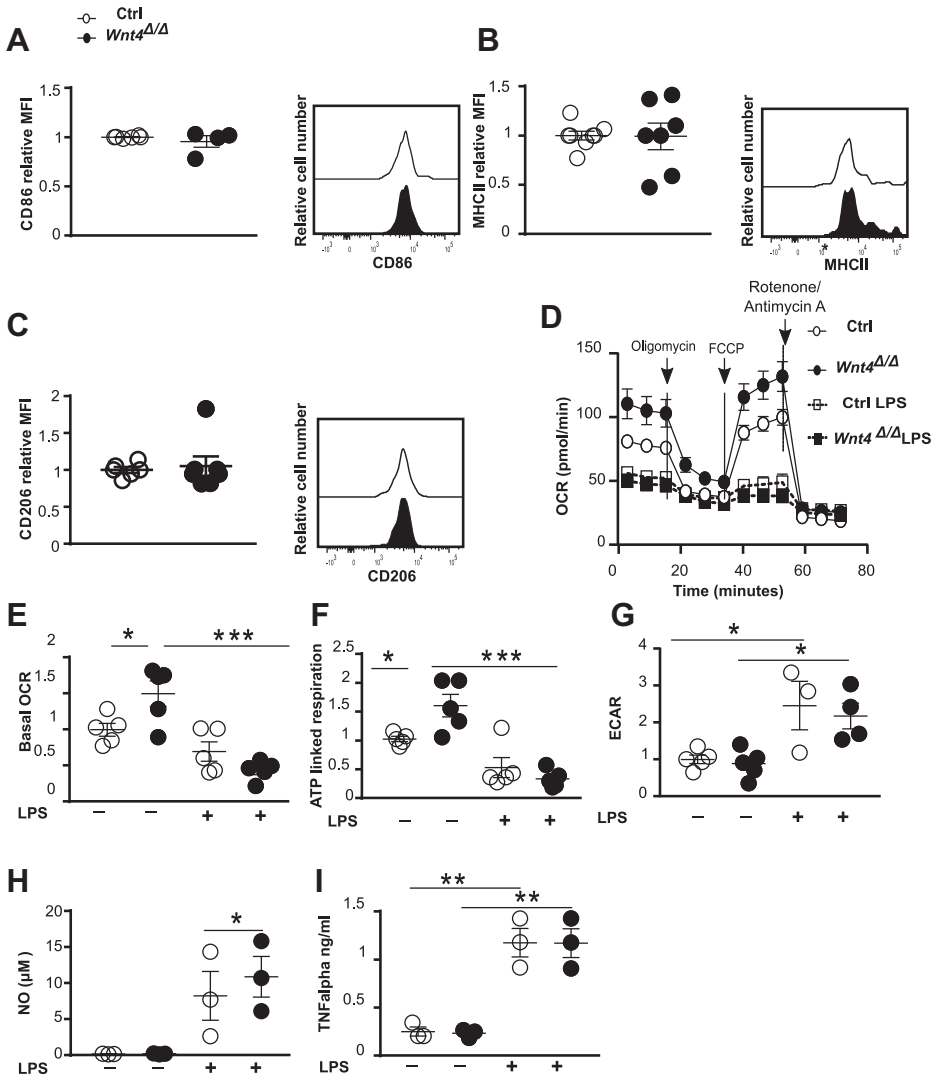

Figure 6. Wnt4$^{\Delta/\Delta}$ BMDM mount strong metabolic and proinflammatory responses to LPS. *A–C*, expression of cell surface markers in BMDM. Relative mean fluorescence intensity (MFI) of CD86 (M1 marker) (*A*), MHCII (M1 Marker) (*B*), and CD206 (M2 Marker) (*C*). *D*, representative oxygen consumption rate (OCR) curves for BMDM pretreated or not with LPS (100 ng/ml). *E–G*, quantification of basal OCR (*E*), ATP-linked respiration (*F*), and extracellular acidification rate (ECAR) (*G*) in BMDM ± LPS. *H*, measure of nitric oxide (NO) in culture supernatants after a 48 h stimulation with LPS. *I*, secretion of TNFα in culture supernatant from cells treated as in *H*. The histograms represent compiled data from three to eight animals per group (mean + SEM). *$p < 0.05$, **$p < 0.01$, ***$p < 0.001$ (two-tailed, unpaired Student's *t* test (two groups) or one-way ANOVA multiple comparisons). BMDM, bone marrow–derived macrophage; LPS, lipopolysaccharide.

Wnt4$^{\Delta/\Delta}$ and control BMDM (Fig. 7, *A* and *B*). However, parasite replication was increased in *Wnt4*$^{\Delta/\Delta}$ BMDM over time (Fig. 7, *A* and *B*). These results indicate that although the metabolic alterations observed in the absence of Wnt4 were not irreversible, *Wnt4*$^{\Delta/\Delta}$ BMDM was more permissive to infection and favored parasite replication. To determine the functional impact of metabolic changes in *Wnt4*$^{\Delta/\Delta}$ BMDM on parasite replication, we treated macrophages with etomoxir to inhibit β-oxidation. Pretreatment with etomoxir had no impact on parasite uptake but resulted in decreased parasite numbers at 72 h in both control and *Wnt4*$^{\Delta/\Delta}$ BMDM (Fig. 7, *B* and *C*). However, etomoxir did not fully rescue *Wnt4*$^{\Delta/\Delta}$ BMDM, suggesting that enhanced β-oxidation is not the only mechanism responsible of the impaired parasite control in *Wnt4*$^{\Delta/\Delta}$ BMDM. Altogether, our results indicate that although the metabolic alterations present in the absence of Wnt4 were not irreversible, enhanced β-oxidation rendered *Wnt4*$^{\Delta/\Delta}$ BMDM more permissive to infection and favored parasite replication.

Discussion

The physiological role of individual Wnt ligands remains enigmatic in a large number of situations due to their often promiscuous signaling. Although the most studied ligands are widely used as prototypes of canonical (Wnt3a) and noncanonical (Wnt5a) Wnt signaling, individual Wnt proteins are often able to activate more than one signaling pathway, depending on cell type and receptor availability (46, 47). We report here a new role for the (mostly) noncanonical ligand Wnt4 in regulating BMDM metabolism. Our results show that Wnt4 regulates mitochondrial ATP production and efficiency without impacting mitochondrial mass. We also demonstrate that PKC-dependent LAL activation results in decreased lipid

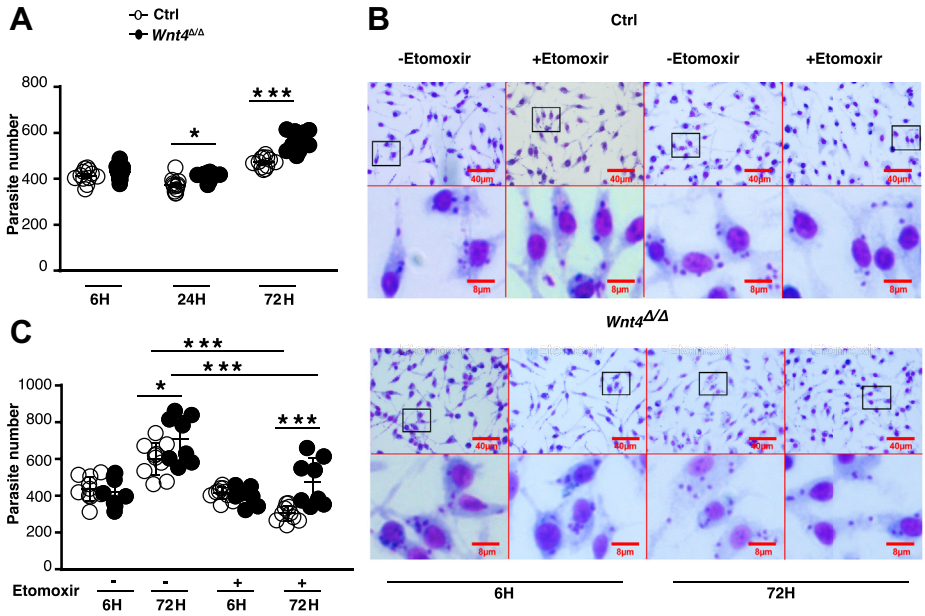

Figure 7. Wnt4 deletion promotes *Leishmania donovani* survival. *A*, parasite numbers per 100 cells as counted from Giemsa-colored slides. *B*, representative microscopy images of infected BMDM at different time points following *L. donovani* infection. *C*, parasite numbers per 100 cells in *L. donovani*-infected cells treated or not with etomoxir, as counted from Giemsa-colored slides. The histograms represent compiled data from five animals per group (mean ± SEM), $*p < 0.05$, $***p < 0.001$ (two-way ANOVA, multiple comparisons). BMDM, bone marrow–derived macrophage.

storage and provides an important fuel for mitochondria in $Wnt4^{\Delta/\Delta}$ BMDM. Wnt4-deficient BMDM was not irreversibly polarized and remained responsive to metabolic reprogramming with LPS. However, enhanced mitochondrial activity and β-oxidation predisposed $Wnt4^{\Delta/\Delta}$ BMDM to infection with the intracellular parasite *L. donovani*, in line with the tenet that macrophage metabolism influences their response to pathogens.

Canonical Wnt/β-catenin signaling is well established in reprogramming tumor cell metabolism toward glycolysis and lactate production instead of mitochondrial OXPHOS (48–51). However, these metabolic trends do not necessarily hold true in nonmalignant context; in fact, stimulation with canonical Wnt ligands increases FAO activity and β-oxidation enzymes in osteoblasts, in contrast to noncanonical ligands, such as Wnt4 (52, 53). It also results in decreased adipogenesis and lipid accumulation in brown adipocytes (53, 54). Our analysis of $Wnt4^{\Delta/\Delta}$ macrophages revealed increased FAO and mitochondrial activity, concomitant with enhanced lipid degradation and decreased lipid storage, thus presenting striking similarities with osteoblasts or adipocytes responding to canonical Wnt signaling. Wnt4 is generally considered a noncanonical Wnt ligand, and its absence could thus result in disinhibition of canonical signals. However, we did not observe significant changes in intracellular phospho-Ser552-β-catenin staining between $Wnt4^{\Delta/\Delta}$ and control macrophages at steady state, and the expression of classical canonical Wnt target genes was downregulated in $Wnt4^{\Delta/\Delta}$ cells. Instead, we showed that the enhanced lipolysis in $Wnt4^{\Delta/\Delta}$ BMDM was dependent on PKC activity and could be further enhanced by the inhibition of PTEN, suggesting that the lack of Wnt4 may promote disinhibition of the noncanonical PKC/Ca^{2+} pathway.

To our knowledge, there are no prior reports on the role of individual Wnt ligands in macrophage metabolism. However, Wnt signaling has been associated with metabolic diseases such obesity, diabetes, and atherosclerosis (55–57). More specifically in macrophages, expression of the canonical Wnt pathway co-receptor low-density lipoprotein (LDL) receptor–related protein was increased after incubation with LDL, and LDL receptor–related protein 5 promoted cholesterol ester accumulation and macrophage transformation to foam cells *in vitro*. LDL-treated macrophages also upregulated canonical Wnt target genes, suggesting an active role for Wnt signaling in this process (58). Conversely, the Wnt antagonist soluble Frizzled-related protein SFRP5 improved glucose tolerance and insulin sensitivity as well as attenuated weight gain in mice on high-fat diet at least in part by inhibiting Wnt5a-dependent activation of inflammatory macrophages *in vivo* (59, 60). Finally, the deletion of β-catenin in macrophages and myeloid cells increases inflammatory responses in macrophages and enhanced the size of atherosclerotic plaques in LDL receptor–deficient mice (61). Wnt4-deficient macrophages displayed an enhanced capacity to degrade lipids, which tempts us to speculate that inhibiting Wnt4 in macrophages could attenuate the impact of high-fat diet on metabolic disorders and atherosclerosis.

ERK and AKT promote the Warburg effect or the preferential generation of ATP *via* lactate production in cancer cells (26, 62–65) by increasing glucose uptake and promoting the activation of glycolytic enzymes (66, 67) (26, 68, 69). Consequently, the attenuated AKT and ERK1/2 activity in $Wnt4^{\Delta/\Delta}$ BMDM should favor OXPHOS instead of lactate production, which is consistent with our analysis. $Wnt4^{\Delta/\Delta}$ BMDM consumes less glucose, and blocking FAO with etomoxir not only restored intracellular lipid droplets but also reverted $Wnt4^{\Delta/\Delta}$

BMDM mitochondrial activity and increased their spare respiratory capacity, indicating a preferential use of lipids as energy source. Enhanced lipid degradation in *Wnt4*$^{\Delta/\Delta}$ cells was chiefly dependent on the activity of lysosomal lipase LAL, with only modest contribution of neutral lipases, such as the adipose triglyceride lipase (ATGL/PNPLA2). Although ATGL is highly expressed in tissue macrophages and its deficiency results in significant lipid droplet accumulation and diminished macrophage function (70, 71), *Pnpla2* was detected at relatively low levels in BMDM in our study, and there was no difference in neutral lipase activity between *Wnt4*$^{\Delta/\Delta}$ and control BMDM.

Wnt4$^{\Delta/\Delta}$ BMDM possessed longer mitochondria with tighter cristae structure, two important determinants of enhanced mitochondrial OXPHOS efficiency (72, 73), but there were no significant changes in the spare respiratory capacity, mitochondrial membrane potential, ROS levels, or mitochondrial mass. These results are consistent with dynamic changes in mitochondrial usage and efficiency as observed upon altered nutrient availability and do not indicate alterations that would permanently rewire mitochondrial function. Taken together, our results indicate that Wnt4 attenuates OXPHOS, likely by regulating mitochondrial connectivity as well as by repressing lipolysis and FAO.

Lipids are important for macrophage function, including phagocytosis, functional polarization, and production of inflammatory mediators (13, 74, 75). Although FAO activity is largely associated with an anti-inflammatory profile (76), *Wnt4*$^{\Delta/\Delta}$ BMDMs are not irreversibly committed. They remain entirely capable of responding to a strong proinflammatory stimulus, such as LPS, and reducing their mitochondrial activity and shifting to glycolysis (76). Their metabolic switch to M_{LPS} was further corroborated by the production of inflammatory mediators, such as NO and TNFα. It should be noted, however, that the BMDM differentiation environment can promote inflammatory polarization (77). Proteomic studies highlighted that the L929 supernatant used here contains secreted factors involved in the regulation of inflammation, such as MIF that modulate the secretion of inflammatory cytokines/interleukins (TNF-α, IFN-γ, IL-2, IL-6, and IL-8) (78) and osteopontin that upregulates IL-12 production (79). Indeed, BMDM differentiated with L929 and stimulated with LPS secrete more TNF-α, IL-6, and IFN-β compared to M-CSF differentiation alone (77), which could potentially influence the polarization we have observed here.

Nevertheless, *Wnt4*$^{\Delta/\Delta}$ BMDM was more permissive to infection by *L. donovani*, and pretreatment of macrophages with etomoxir resulted in decreased parasite replication, demonstrating that elevated β-oxidation in *Wnt4*$^{\Delta/\Delta}$ cells was at least partially responsible. Macrophages are the natural mammalian host cells for *Leishmania* parasites, and the pathogen has developed multiple strategies to evade their microbicidal effects (80, 81). One such strategy *in vivo* is the generation of monocyte-derived myeloid cells with altered function that will promote parasite growth (82, 83). Our results are well in line with this theory and demonstrate that the metabolic alterations in *Wnt4*$^{\Delta/\Delta}$ BMDM have functional consequences. *L. donovani* infection has also been shown to decrease Wnt5a expression in BMDM at gene and protein levels. Conversely, exogenous Wnt5a decreased parasite burden *via* activation of Rac/Rho GTPases, while Wnt5a knockdown by siRNA prior to infection increased parasite survival (84). Our results phenocopy the impact of Wnt5a deletion on parasite replication. More importantly, our data connect Wnt signaling, β-oxidation, and mitochondrial activity in *L. donovani* survival, thus highlighting the importance of macrophage metabolism to the outcome of host–parasite interactions.

In conclusion, our results identify a cell-intrinsic role for Wnt4 in regulating macrophage metabolism. Wnt4 deficiency disturbs energy homeostasis by increasing mitochondrial ATP levels mainly through FAO. Although Wnt4-deficient macrophages demonstrate a strong proinflammatory response to LPS, they were more susceptible to support the growth of an intracellular pathogen. These results demonstrate that noncanonical Wnt4 signaling regulates macrophage function and modulates their metabolism in a context-dependent manner. Further mechanistic and metabolic investigations may be helpful to identify how the Wnt4 pathway could be best harnessed to promote the control of intracellular infections or to modulate macrophage function in the context of metabolic disorders.

Experimental procedures

Experimental animals

B6.129P2-Lyz2$^{tm1(cre)Ifo}$/J (LysMCre) mice were purchased from The Jackson Laboratory. Mice with a *Wnt4* conditional allele have been described elsewhere (85) and were originally a kind gift from S. Vainio (Oulu University, Finland). Mice were bred and housed under specific pathogen-free conditions in sterile ventilated racks at the animal facility of INRS-Centre Armand-Frappier Santé Biotechnologie. All procedures were approved by the Comité institutionnel de la protection des animaux of the INRS and were conducted in accordance with the Canadian Council on Animal Care guidelines. Only female mice were used for the following experiments.

Flow cytometry analysis

BM was harvested by flushing tibias and femurs with PBS/0.1% BSA/0.5 mmol EDTA using a 25-gauge needle. To analyze BMDM, the following antibodies were used: anti-CD11c, anti-Ly6C, anti-F4/80, anti-MHCII, anti-CD206, anti-CD86 (BD Biosciences). For intracellular staining, surface-stained BM cells were fixed and permeabilized using the Foxp3 staining kit (eBioscience) and then incubated with the following primary antibodies: Arg1 (R&D Systems, PE-conjugated), iNOS (eBioscience, APC-conjugated), p-AKT(Thr308) (1/100), p-AKT (Ser473) (1/100), β-catenin (Ser552) 1/200), p-ERK (Thr202/Tyr204)(1/100), ERK (1/100), AKT (1/100), p-JNK (1/100), JNK (1/100), p-S6 (Ser235/236), p-4E-BP1 (Thr37/46) (all from Cell Signaling Technologies), or Lamp1 (1/800) (Abcam), overnight at 4 °C; or conjugated Ki-67 (FITC) for 1 h at room temperature. Unconjugated

antibodies were detected with an Alexa 488-conjugated $F(ab')_2$ fragment against rabbit IgG (Molecular Probes). The stained cells were analyzed on a four-laser BD LSRFortessa cell analyzer (BD Biosciences) and analyzed using FACS DiVa (v. 8.1) or FlowJo (v. 10.1) software.

Cell culture

BM was flushed with 5 ml Hank's Balanced Salt Solution (HBSS), centrifuged at 1236*g* or 7 min, and the pellet was resuspended in Dulbecco's modified Eagle's medium (DMEM) (Life Technologies) supplemented with 10% fetal bovine serum (FBS Premium, Wisent Bioproducts) at 5×10^6 cell/ml. 1.5×10^6 cells were seeded in a nonadherent Petri dish and cultured in DMEM supplemented with 10% FBS and 20% conditioned medium from L929 fibroblasts as previously described (86). The differentiation medium was refreshed on day 5, and adherent BMDMs were collected with Trypsin/EDTA solution on day 7 and analyzed by flow cytometry or replated in DMEM/10% FBS for further analyses. LPS was purchased from Sigma-Aldrich and used at a final concentration of 100 ng/ml. Oligomycin was (2 μM) (Sigma Aldrich) was added for 1 h at 37 °C. For autophagy induction, BMDMs were replated in Earle's Balanced Salt Solution (Life Technologies) for 2 h at 37 °C with or without Bafilomycin (100 nM).

Immunofluorescence

2×10^5 cells were seeded overnight on uncoated coverslips at 37 °C. The cells were first fixed with 4% paraformaldehyde for 15 min at room temperature and then washed three times with PBS. Fixed BMDM were permeabilized with PBS/0.1% Triton X-100 solution, for 2 min, then blocked with PBS/0.1% Triton/1% BSA for 10 min. The cells were incubated for 1 h at room temperature with primary antibodies: anti-LC3 (1/100) (Cell Signaling Technologies) or anti-Tom20 (1/100) (Abcam), washed three times with PBS, and incubated with Alexa 488-conjugated secondary antibody (1/1000) for 30 min at room temperature. Finally, the coverslips were washed and mounted on the microscope slides with ProLong Diamond Antifade Mountant with DAPI (Thermo Fisher Scientific). Images were taken using a LSM 780 confocal microscope with 60× oil objective.

Enzymatic activity

Cathepsin B activity: Cells were collected with Trypsin with 0.25% EDTA, washed with PBS 1×, and collected by centrifugation at 200*g* for 5 min, at 4 °C. Cells were lysed by buffer containing Tris-HCL 50 mM, NaCl 150 mM, EDTA 1 mM, and Triton X-100 (0.5%) and centrifuged at 18,300*g* for 12 min at 4 °C. Supernatants were collected, and proteins were dosed with Bradford Kit (Bio-Rad). Proteins (10 μg) were diluted in 100 μl of 100 mM Hepes, pH 6.0, 150 mM NaCl, 2 mM DTT, and 5 mM EDTA in the presence of a 5 μM concentration of the cathepsin B substrate zRR-AMC (Sigma-Aldrich). Samples were incubated for 30 min at 37 °C, and fluorescence was measured (excitation/emission 360/440 nm) using a Cytation5 Cell Imaging Multi-Mode Reader.

LAL activity was measured as described (87) by diluting 20 μg of proteins from each samples treated with GF109203X (PKC inhibitor) at 5 μM for 1 h at 37 °C or with bpV(pic) (PTEN inhibitor) at 1 μM for 2 h at 37 °C or controls in 100 μl of reaction buffer (100 mM sodium acetate, pH 4.0, 1% (v/v) Triton X-100, and 0.5% (w/v) cardiolipin) in the presence of 0.345 mM 4-methylumbelliferone (Sigma-Aldrich). Samples were incubated for 1 h at 37 °C. Fluorescence was measured (excitation/emission 360/440 nm) using a Cytation5 Cell Imaging Multi-Mode Reader.

Citrate synthase: Citrate Synthase Activity Colorimetric Assay Kit (BioVision, Catalog # K318–100), following manufacturer's instructions.

ATP and lactate assays

2×10^5 cells were grown in 96-well plates. Cellular ATP was measured by ATP using Cell Titer Glow kit (Promega), and total lactate was measured using Lactate Colorimetric/Fluorometric (BioVision) Assay Kit and was measured in triplicate following the protocol provided.

Elisa TNFα

Supernatants were collected from Wnt4Δ/Δ BMDM and control cultures upon 6 h stimulation with LPS and at 6 h, 24 h, and 72 h postinfection with *L. donovani*. 50 μl from each condition were added in duplicates, and TNFα levels were measured using Mouse TNF-alpha Quantikine ELISA Kit (R&D SYSTEMS, Catalog # MTA00B) as per manufacturer's instructions.

Nitric oxide quantification

Supernatants were collected from $Wnt4^{\Delta/\Delta}$ BMDM and control cultures upon 24 h stimulation with LPS and at 6 h, 24 h, and 72 h postinfection with *L. donovani*. 100 μl from each condition were added in duplicates to 96-well plates. Nitrate levels were measured by the Greiss reaction, as described in (88, 89).

Glucose consumption

Supernatants were collected from Wnt4Δ/Δ BMDM and control cultures. 50 μl from each condition were added in duplicates to 96-well plates, and glucose levels were determined using Glucose Colorimetric/Fluorometric Assay Kit (BioVision, Catalog # K606–100) as per manufacturer's instructions.

MitoSOX

BMDMs were collected and stained with the MitoSOX Red mitochondrial superoxide indicator reagent (Invitrogen) at a final concentration of 5 μM, and the cells were incubated for 30 min at 37 °C, after which they were washed and analyzed by for flow cytometry.

Tetramethylrhodamine methyl ester

BMDMs were collected and stained with tetramethylrhodamine methyl ester (Thermo Fisher) at a final concentration 0.5 nM, and the cells were incubated for 30 min at 37 ºC, after which they were washed and analyzed by for flow cytometry.

Extracellular flux analysis

BMDMs were seeded at 4×10^4 cells on Seahorse XF96 cell culture microplates (Agilent) and treated with etomoxir (250 μM) and 2-DG (5 mM) for 30 min at 37 °C. Medium was changed with Seahorse XF DMEM medium, pH 7.4 (Agilent) supplemented with 10 Mm glucose, 1 Mm pyruvate, and 2 mM glutamine, and cells were incubated for 1 h at 37 °C with no CO2. Mito stress kit (Agilent) was used, and XF analysis was performed using the XFe-96 analyzer (Seahorse Bioscience) as per manufacturer's instructions. All reagents provided by Sigma-Aldrich.

qRT-PCR

Cells were collected from BMDM differentiation after 7 days in culture. The manufacturer's protocol was followed for total RNA extraction. RNAEasy columns (Qiagen) were used to concentrate and clean the preparation. High-capacity cDNA reverse transcription kit (Applied Biosystems) was used to convert total RNA to cDNA. TaqMan custom PreAmp kit (Applied Biosystems) was used to pre-amplified the cDNA product. Quantitative RT-PCR was performed using TaqMan reagents and assays (TBP; and B2m; as an internal control, from Applied Biosystems) on Stratagene M x x3000P instrument. Relative quantification of Wnt4 was determined by using the ΔΔCT method.

L. donovani *culture and infections*

Promastigotes of L. *donovani* (MHOM/ET/67/Hu3:LV9) freshly differentiated from splenic amastigotes were cultured in Leishmania medium (M199 medium supplemented with 10% heat-inactivated FBS (Hyclone), 100 μM hypoxanthine, 10 mM Hepes, 5 μM hemin, 3 μM biopterin, 1 μM biotin, penicillin (100 I.U./ml), and streptomycin (100 μg/ml)) at 26 °C. For BMDM infections, metacyclic promastigotes were isolated at 1400 RPM in 15-ml Falcon conical centrifuge tubes containing 1 ml of 40% Ficoll (GE Healthcare) at the bottom, overlaid by 2 ml of a single gradient of 10% Ficoll and overlay 1×10^8 promastigotes from the late stationary growth phase in 2 ml of nonsupplemented DMEM (90). Complement opsonization of metacyclic promastigotes was performed prior to infections by incubating the parasites in HBSS containing 10% serum from DBA/2 mice for 30 min at 37 °C. BMDMs were then incubated at 37 °C with metacyclic promastigotes (parasite-to-macrophage ratio of 5:1). After 3 h of incubation, noninternalized parasites were washed 3× with warm HBSS. The time points are described in each experiment. Infection levels were assessed by microscopic examination of infected cells after Giemsa staining with the Hema 3 system (Fisher Scientific).

Western blot

Cells were collected with trypsin with 0.25% EDTA, washed with PBS 1×, and collected by centrifugation at 200*g* for 5 min, at 4 °C, cells were lysed by buffer containing Tris-HCL 50 mM, NaCl 150 mM, EDTA 1 mM, and Triton 0.5%, and centrifuge at 18,300*g* for 12 min, at 4 °C. Supernatants were collected, and phosphatase (NAF 0.3 mM) inhibitor was added. Proteins were dosed with Bradford Kit (Biorad). Prior to electrophoresis, samples were mixed with loading buffer to obtain 1× and 5% β-mercaptophenol (62.5 mM Tris-HCl pH 6.5, 2.5% SDS, 10% glycerol, 0.01% bromophenol blue) and incubated at 95 °C for 5 min. Proteins (50 μg) were added to each well, then resolved on SDS-PAGE followed by wet-transfer to PVDF membranes. Detection was done by immunoblotting using the indicated antibody, Tom20 (Abcam1/1000). The membrane was developed on the automatic film processor machine (AFP ImageWorks).

Statistical analysis

Each value represents at least three independent experiments. Two-tailed Student *t* test or ordinary one-way ANOVA or two-way ANOVA were used as indicated in figure legends to determine statistical significance. A p value < 0.05 was considered significant.

Data availability

All data presented in the manuscript are contained within the manuscript. Additional information will be shared upon reasonable request to the corresponding author, Krista Heinonen. krista.heinonen@inrs.ca

Supporting information—This article contains supporting information, providing additional characterization of Wnt4-deficient BMDM.

Author contributions—M. T., M. G., and K. M. H. conceptualization; M. T. formal analysis; M. T., H. A. investigation; M. T. visualization; M. T. writing–original draft; A. D., M. G., and K. M. H. resources; A. D., M. G., and K. M. H. writing–review & editing; K. M. H. funding acquisition; K. M. H. supervision.

Funding and additional information—This work was supported by the Natural Sciences and Engineering Research Council of Canada (NSERC Discovery grants #419226–2012 and #2018–05258 to K. M. H.). K. M. H. is a FRQS Junior Research Scholar. A.D. holds the Canada Research Chair on the Biology of intracellular parasitism.

Conflict of interest—The authors declare that they have no conflicts of interest with the contents of this article.

Abbreviations—The abbreviations used are: BMDM, bone marrow–derived macrophage; DMEM, Dulbecco's modified Eagle's medium; ERK1/2, extracellular signal–regulated kinases 1 and 2; FA, fatty acid; FAO, fatty acid oxidation; FBS, fetal bovine serum; HBSS, Hank's Balanced Salt Solution; JNK, c-Jun N-terminal protein kinase; LAL, lysosomal acid lipase; LPS, lipopolysaccharide; M1, classically activated proinflammatory macrophages; M2, alternatively activated anti-inflammatory macrophages; MAPK, mitogen-

activated protein kinase; OXPHOS, oxidative phosphorylation; OCR, oxygen consumption rates.

References

1. Hirayama, D., Iida, T., and Nakase, H. (2017) The phagocytic function of macrophage-enforcing innate immunity and tissue homeostasis. *Int. J. Mol. Sci.* **19**, 92
2. Gordon, S., and Pluddemann, A. (2017) Tissue macrophages: heterogeneity and functions. *BMC Biol.* **15**, 53
3. Wang, C., Yu, X., Cao, Q., Wang, Y., Zheng, G., Tan, T. K., *et al.* (2013) Characterization of murine macrophages from bone marrow, spleen and peritoneum. *BMC Immunol.* **14**, 6
4. Mills, C. D., Kincaid, K., Alt, J. M., Heilman, M. J., and Hill, A. M. (2000) M-1/M-2 macrophages and the Th1/Th2 paradigm. *J. Immunol.* **164**, 6166–6173
5. Italiani, P., and Boraschi, D. (2014) From monocytes to M1/M2 macrophages: phenotypical vs. Functional differentiation. *Front. Immunol.* **5**, 514
6. Van Ginderachter, J. A., Movahedi, K., Hassanzadeh Ghassabeh, G., Meerschaut, S., Beschin, A., Raes, G., *et al.* (2006) Classical and alternative activation of mononuclear phagocytes: picking the best of both worlds for tumor promotion. *Immunobiology* **211**, 487–501
7. Ley, K. (2017) M1 means kill; M2 means heal. *J. Immunol.* **199**, 2191–2193
8. Jha, A. K., Huang, S. C., Sergushichev, A., Lampropoulou, V., Ivanova, Y., Loginicheva, E., *et al.* (2015) Network integration of parallel metabolic and transcriptional data reveals metabolic modules that regulate macrophage polarization. *Immunity* **42**, 419–430
9. Artyomov, M. N., Sergushichev, A., and Schilling, J. D. (2016) Integrating immunometabolism and macrophage diversity. *Semin. Immunol.* **28**, 417–424
10. Liu, L., Lu, Y., Martinez, J., Bi, Y., Lian, G., Wang, T., *et al.* (2016) Proinflammatory signal suppresses proliferation and shifts macrophage metabolism from Myc-dependent to HIF1alpha-dependent. *Proc. Natl. Acad. Sci. U. S. A.* **113**, 1564–1569
11. Kelly, B., and O'Neill, L. A. (2015) Metabolic reprogramming in macrophages and dendritic cells in innate immunity. *Cell Res.* **25**, 771–784
12. Nomura, M., Liu, J., Rovira, , II, Gonzalez-Hurtado, E., Lee, J., Wolfgang, M. J., *et al.* (2016) Fatty acid oxidation in macrophage polarization. *Nat. Immunol.* **17**, 216–217
13. Huang, S. C., Everts, B., Ivanova, Y., O'Sullivan, D., Nascimento, M., Smith, A. M., *et al.* (2014) Cell-intrinsic lysosomal lipolysis is essential for alternative activation of macrophages. *Nat. Immunol.* **15**, 846–855
14. Malsin, E. S., Kim, S., Lam, A. P., and Gottardi, C. J. (2019) Macrophages as a source and recipient of Wnt signals. *Front. Immunol.* **10**, 1813
15. Neumann, J., Schaale, K., Farhat, K., Endermann, T., Ulmer, A. J., Ehlers, S., *et al.* (2010) Frizzled1 is a marker of inflammatory macrophages, and its ligand Wnt3a is involved in reprogramming Mycobacterium tuberculosis-infected macrophages. *FASEB J.* **24**, 4599–4612
16. Schaale, K., Neumann, J., Schneider, D., Ehlers, S., and Reiling, N. (2011) Wnt signaling in macrophages: augmenting and inhibiting mycobacteria-induced inflammatory responses. *Eur. J. Cel. Biol.* **90**, 553–559
17. Naskar, D., Maiti, G., Chakraborty, A., Roy, A., Chattopadhyay, D., and Sen, M. (2014) Wnt5a-Rac1-NF-kappaB homeostatic circuitry sustains innate immune functions in macrophages. *J. Immunol.* **192**, 4386–4397
18. Heinonen, K. M., Vanegas, J. R., Lew, D., Krosl, J., and Perreault, C. (2011) Wnt4 enhances murine hematopoietic progenitor cell expansion through a planar cell polarity-like pathway. *PLoS One* **6**, e19279
19. Hung, L. Y., Johnson, J. L., Ji, Y., Christian, D. A., Herbine, K. R., Pastore, C. F., *et al.* (2019) Cell-intrinsic Wnt4 influences conventional dendritic cell fate determination to suppress type 2 immunity. *J. Immunol.* **203**, 511–519
20. Hung, L. Y., Sen, D., Oniskey, T. K., Katzen, J., Cohen, N. A., Vaughan, A. E., *et al.* (2019) Macrophages promote epithelial proliferation following infectious and non-infectious lung injury through a Trefoil factor 2-dependent mechanism. *Mucosal Immunol.* **12**, 64–76
21. Yu, B., Chang, J., Liu, Y., Li, J., Kevork, K., Al-Hezaimi, K., *et al.* (2014) Wnt4 signaling prevents skeletal aging and inflammation by inhibiting nuclear factor-kappaB. *Nat. Med.* **20**, 1009–1017
22. Cross, M., Mangelsdorf, I., Wedel, A., and Renkawitz, R. (1988) Mouse lysozyme M gene: isolation, characterization, and expression studies. *Proc. Natl. Acad. Sci. U. S. A.* **85**, 6232–6236
23. Clausen, B. E., Burkhardt, C., Reith, W., Renkawitz, R., and Forster, I. (1999) Conditional gene targeting in macrophages and granulocytes using LysMcre mice. *Transgenic Res.* **8**, 265–277
24. Hetu-Arbour, R., Tlili, M., Bandeira Ferreira, F. L., Abidin, B. M., Kwarteng, E. O., and Heinonen, K. M. (2021) Cell-intrinsic Wnt4 promotes hematopoietic stem and progenitor cell self-renewal. *Stem Cells* **39**, 1207–1220
25. Traves, P. G., de Atauri, P., Marin, S., Pimentel-Santillana, M., Rodriguez-Prados, J. C., Marin de Mas, I., *et al.* (2012) Relevance of the MEK/ERK signaling pathway in the metabolism of activated macrophages: a metabolomic approach. *J. Immunol.* **188**, 1402–1410
26. Papa, S., Choy, P. M., and Bubici, C. (2019) The ERK and JNK pathways in the regulation of metabolic reprogramming. *Oncogene* **38**, 2223–2240
27. Yu, J. S., and Cui, W. (2016) Proliferation, survival and metabolism: the role of PI3K/AKT/mTOR signalling in pluripotency and cell fate determination. *Development* **143**, 3050–3060
28. Altomare, D. A., and Khaled, A. R. (2012) Homeostasis and the importance for a balance between AKT/mTOR activity and intracellular signaling. *Curr. Med. Chem.* **19**, 3748–3762
29. Cargnello, M., and Roux, P. P. (2011) Activation and function of the MAPKs and their substrates, the MAPK-activated protein kinases. *Microbiol. Mol. Biol. Rev.* **75**, 50–83
30. Remmerie, A., and Scott, C. L. (2018) Macrophages and lipid metabolism. *Cell Immunol.* **330**, 27–42
31. Singh, R. K., Barbosa-Lorenzi, V. C., Lund, F. W., Grosheva, I., Maxfield, F. R., and Haka, A. S. (2016) Degradation of aggregated LDL occurs in complex extracellular sub-compartments of the lysosomal synapse. *J. Cel. Sci.* **129**, 1072–1082
32. Ouimet, M., Franklin, V., Mak, E., Liao, X., Tabas, I., and Marcel, Y. L. (2011) Autophagy regulates cholesterol efflux from macrophage foam cells *via* lysosomal acid lipase. *Cell Metab.* **13**, 655–667
33. Van den Bossche, J., Baardman, J., and de Winther, M. P. (2015) Metabolic characterization of polarized M1 and M2 bone marrow-derived macrophages using real-time extracellular flux analysis. *JoVE* **28**, 53424
34. Ishitani, T., Kishida, S., Hyodo-Miura, J., Ueno, N., Yasuda, J., Waterman, M., *et al.* (2003) The TAK1-NLK mitogen-activated protein kinase cascade functions in the Wnt-5a/Ca(2+) pathway to antagonize Wnt/beta-catenin signaling. *Mol. Cell. Biol.* **23**, 131–139
35. Valledor, A. F., Xaus, J., Marques, L., and Celada, A. (1999) Macrophage colony-stimulating factor induces the expression of mitogen-activated protein kinase phosphatase-1 through a protein kinase C-dependent pathway. *J. Immunol.* **163**, 2452–2462
36. Ries, S., Buchler, C., Langmann, T., Fehringer, P., Aslanidis, C., and Schmitz, G. (1998) Transcriptional regulation of lysosomal acid lipase in differentiating monocytes is mediated by transcription factors Sp1 and AP-2. *J. Lipid Res.* **39**, 2125–2134
37. Wolf, A. M., Lyuksyutova, A. I., Fenstermaker, A. G., Shafer, B., Lo, C. G., and Zou, Y. (2008) Phosphatidylinositol-3-kinase-atypical protein kinase C signaling is required for Wnt attraction and anterior-posterior axon guidance. *J. Neurosci.* **28**, 3456–3467
38. Pearn, L., Fisher, J., Burnett, A. K., and Darley, R. L. (2007) The role of PKC and PDK1 in monocyte lineage specification by Ras. *Blood* **109**, 4461–4469
39. Namgaladze, D., and Brune, B. (2016) Macrophage fatty acid oxidation and its roles in macrophage polarization and fatty acid-induced inflammation. *Biochim. Biophys. Acta* **1861**, 1796–1807
40. Cavallo-Medved, D., Moin, K., and Sloane, B. (2011) Cathepsin B: basis sequence: mouse. *The AFCS-Nature Mol. Pages* **2011**, A000508
41. Oelschlaegel, D., Weiss Sadan, T., Salpeter, S., Krug, S., Blum, G., Schmitz, W., *et al.* (2020) Cathepsin inhibition modulates metabolism and polarization of tumor-associated macrophages. *Cancers* **12**, 2579

42. Park, B. S., and Lee, J. O. (2013) Recognition of lipopolysaccharide pattern by TLR4 complexes. *Exp. Mol. Med.* **45**, e66
43. Liu, D., and Uzonna, J. E. (2012) The early interaction of Leishmania with macrophages and dendritic cells and its influence on the host immune response. *Front. Cell. Infect. Microbiol.* **2**, 83
44. Tomiotto-Pellissier, F., Bortoleti, B., Assolini, J. P., Goncalves, M. D., Carloto, A. C. M., Miranda-Sapla, M. M., *et al.* (2018) Macrophage polarization in leishmaniasis: broadening horizons. *Front. Immunol.* **9**, 2529
45. Podinovskaia, M., and Descoteaux, A. (2015) Leishmania and the macrophage: a multifaceted interaction. *Future Microbiol.* **10**, 111–129
46. Mikels, A. J., and Nusse, R. (2006) Purified Wnt5a protein activates or inhibits beta-catenin-TCF signaling depending on receptor context. *PLoS Biol.* **4**, e115
47. Grumolato, L., Liu, G., Mong, P., Mudbhary, R., Biswas, R., Arroyave, R., *et al.* (2010) Canonical and noncanonical Wnts use a common mechanism to activate completely unrelated coreceptors. *Genes Dev.* **24**, 2517–2530
48. Pate, K. T., Stringari, C., Sprowl-Tanio, S., Wang, K., TeSlaa, T., Hoverter, N. P., *et al.* (2014) Wnt signaling directs a metabolic program of glycolysis and angiogenesis in colon cancer. *EMBO J.* **33**, 1454–1473
49. Zhuang, X., Zhang, H., Li, X., Li, X., Cong, M., Peng, F., *et al.* (2017) Differential effects on lung and bone metastasis of breast cancer by Wnt signalling inhibitor DKK1. *Nat. Cel. Biol.* **19**, 1274–1285
50. Mendez-Lucas, A., Li, X., Hu, J., Che, L., Song, X., Jia, J., *et al.* (2017) Glucose catabolism in liver tumors induced by c-MYC can be sustained by various PKM1/PKM2 ratios and pyruvate kinase activities. *Cancer Res.* **77**, 4355–4364
51. Chafey, P., Finzi, L., Boisgard, R., Cauzac, M., Clary, G., Broussard, C., *et al.* (2009) Proteomic analysis of beta-catenin activation in mouse liver by DIGE analysis identifies glucose metabolism as a new target of the Wnt pathway. *Proteomics* **9**, 3889–3900
52. Frey, J. L., Kim, S. P., Li, Z., Wolfgang, M. J., and Riddle, R. C. (2018) Beta-catenin directs long-chain fatty acid catabolism in the osteoblasts of male mice. *Endocrinology* **159**, 272–284
53. Frey, J. L., Li, Z., Ellis, J. M., Zhang, Q., Farber, C. R., Aja, S., *et al.* (2015) Wnt-Lrp5 signaling regulates fatty acid metabolism in the osteoblast. *Mol. Cell. Biol.* **35**, 1979–1991
54. Kang, S., Bajnok, L., Longo, K. A., Petersen, R. K., Hansen, J. B., Kristiansen, K., *et al.* (2005) Effects of Wnt signaling on brown adipocyte differentiation and metabolism mediated by PGC-1alpha. *Mol. Cell. Biol.* **25**, 1272–1282
55. Du, J., and Li, J. (2018) The role of Wnt signaling pathway in atherosclerosis and its relationship with angiogenesis. *Exp. Ther. Med.* **16**, 1975–1981
56. Bordonaro, M. (2009) Role of Wnt signaling in the development of type 2 diabetes. *Vitamins Horm.* **80**, 563–581
57. Chen, N., and Wang, J. (2018) Wnt/beta-Catenin signaling and obesity. *Front. Physiol.* **9**, 792
58. Borrell-Pages, M., Romero, J. C., Juan-Babot, O., and Badimon, L. (2011) Wnt pathway activation, cell migration, and lipid uptake is regulated by low-density lipoprotein receptor-related protein 5 in human macrophages. *Eur. Heart J.* **32**, 2841–2850
59. Au, D. T., Migliorini, M., Strickland, D. K., and Muratoglu, S. C. (2018) Macrophage LRP1 promotes diet-induced hepatic inflammation and metabolic dysfunction by modulating Wnt signaling. *Med. Inflamm.* **2018**, 7902841
60. Ouchi, N., Higuchi, A., Ohashi, K., Oshima, Y., Gokce, N., Shibata, R., *et al.* (2010) Sfrp5 is an anti-inflammatory adipokine that modulates metabolic dysfunction in obesity. *Science* **329**, 454–457
61. Wang, F., Liu, Z., Park, S. H., Gwag, T., Lu, W., Ma, M., *et al.* (2018) Myeloid beta-catenin deficiency exacerbates atherosclerosis in low-density lipoprotein receptor-deficient mice. *Arteriosclerosis, Thromb. Vasc. Biol.* **38**, 1468–1478
62. Chen, X. S., Li, L. Y., Guan, Y. D., Yang, J. M., and Cheng, Y. (2016) Anticancer strategies based on the metabolic profile of tumor cells: therapeutic targeting of the Warburg effect. *Acta Pharmacol. Sinica* **37**, 1013–1019
63. Danhier, P., Banski, P., Payen, V. L., Grasso, D., Ippolito, L., Sonveaux, P., *et al.* (2017) Cancer metabolism in space and time: beyond the Warburg effect. *Biochim. Biophys. Acta Bioenerg.* **1858**, 556–572
64. Cassim, S., Vucetic, M., Zdralevic, M., and Pouyssegur, J. (2020) Warburg and beyond: the power of mitochondrial metabolism to collaborate or replace fermentative glycolysis in cancer. *Cancers* **12**, 1119
65. Hsu, P. P., and Sabatini, D. M. (2008) Cancer cell metabolism: warburg and beyond. *Cell* **134**, 703–707
66. Elstrom, R. L., Bauer, D. E., Buzzai, M., Karnauskas, R., Harris, M. H., Plas, D. R., *et al.* (2004) Akt stimulates aerobic glycolysis in cancer cells. *Cancer Res.* **64**, 3892–3899
67. Gottlob, K., Majewski, N., Kennedy, S., Kandel, E., Robey, R. B., and Hay, N. (2001) Inhibition of early apoptotic events by Akt/PKB is dependent on the first committed step of glycolysis and mitochondrial hexokinase. *Genes Dev.* **15**, 1406–1418
68. Zhang, Z., Deng, X., Liu, Y., Liu, Y., Sun, L., and Chen, F. (2019) PKM2, function and expression and regulation. *Cell Biosci.* **9**, 52
69. Yang, W., Zheng, Y., Xia, Y., Ji, H., Chen, X., Guo, F., *et al.* (2012) ERK1/2-dependent phosphorylation and nuclear translocation of PKM2 promotes the Warburg effect. *Nat. Cel. Biol.* **14**, 1295–1304
70. Lammers, B., Chandak, P. G., Aflaki, E., Van Puijvelde, G. H., Radovic, B., Hildebrand, R. B., *et al.* (2011) Macrophage adipose triglyceride lipase deficiency attenuates atherosclerotic lesion development in low-density lipoprotein receptor knockout mice. *Arteriosclerosis, Thromb. Vasc. Biol.* **31**, 67–73
71. Chandak, P. G., Radovic, B., Aflaki, E., Kolb, D., Buchebner, M., Frohlich, E., *et al.* (2010) Efficient phagocytosis requires triacylglycerol hydrolysis by adipose triglyceride lipase. *J. Biol. Chem.* **285**, 20192–20201
72. Trevisan, T., Pendin, D., Montagna, A., Bova, S., Ghelli, A. M., and Daga, A. (2018) Manipulation of mitochondria dynamics reveals separate roles for form and function in mitochondria distribution. *Cell Rep.* **23**, 1742–1753
73. Cogliati, S., Frezza, C., Soriano, M. E., Varanita, T., Quintana-Cabrera, R., Corrado, M., *et al.* (2013) Mitochondrial cristae shape determines respiratory chain supercomplexes assembly and respiratory efficiency. *Cell* **155**, 160–171
74. Yan, J., and Horng, T. (2020) Lipid metabolism in regulation of macrophage functions. *Trends Cell Biol.* **30**, 979–989
75. Cader, M. Z., Boroviak, K., Zhang, Q., Assadi, G., Kempster, S. L., Sewell, G. W., *et al.* (2016) C13orf31 (FAMIN) is a central regulator of immunometabolic function. *Nat. Immunol.* **17**, 1046–1056
76. Van den Bossche, J., O'Neill, L. A., and Menon, D. (2017) Macrophage immunometabolism: where are we (going)? *Trends Immunol.* **38**, 395–406
77. Heap, R. E., Marin-Rubio, J. L., Peltier, J., Heunis, T., Dannoura, A., Moore, A., *et al.* (2021) Proteomics characterisation of the L929 cell supernatant and its role in BMDM differentiation. *Life Sci. Alliance* **4**, e202000957
78. Calandra, T., and Roger, T. (2003) Macrophage migration inhibitory factor: a regulator of innate immunity. *Nat. Rev. Immunol.* **3**, 791–800
79. Clemente, N., Raineri, D., Cappellano, G., Boggio, E., Favero, F., Soluri, M. F., *et al.* (2016) Osteopontin bridging innate and adaptive immunity in autoimmune diseases. *J. Immunol. Res.* **2016**, 7675437
80. Muxel, S. M., Aoki, J. I., Fernandes, J. C. R., Laranjeira-Silva, M. F., Zampieri, R. A., Acuna, S. M., *et al.* (2017) Arginine and polyamines fate in Leishmania infection. *Front. Microbiol.* **8**, 2682
81. Arango Duque, G., and Descoteaux, A. (2014) Macrophage cytokines: involvement in immunity and infectious diseases. *Front. Immunol.* **5**, 491
82. Abidin, B. M., Hammami, A., Stager, S., and Heinonen, K. M. (2017) Infection-adapted emergency hematopoiesis promotes visceral leishmaniasis. *PLoS Pathog.* **13**, e1006422
83. Hammami, A., Abidin, B. M., Charpentier, T., Fabie, A., Duguay, A. P., Heinonen, K. M., *et al.* (2017) HIF-1alpha is a key regulator in potentiating suppressor activity and limiting the microbicidal capacity of MDSC-like cells during visceral leishmaniasis. *PLoS Pathog.* **13**, e1006616
84. Chakraborty, A., Kurati, S. P., Mahata, S. K., Sundar, S., Roy, S., and Sen, M. (2017) Wnt5a signaling promotes host defense against Leishmania donovani infection. *J. Immunol.* **199**, 992–1002

85. Shan, J., Jokela, T., Peltoketo, H., and Vainio, S. (2009) Generation of an allele to inactivate Wnt4 gene function conditionally in the mouse. *Genesis* **47**, 782–788
86. Heinonen, K. M., Dube, N., Bourdeau, A., Lapp, W. S., and Tremblay, M. L. (2006) Protein tyrosine phosphatase 1B negatively regulates macrophage development through CSF-1 signaling. *Proc. Natl. Acad. Sci. U. S. A.* **103**, 2776–2781
87. Dairaku, T., Iwamoto, T., Nishimura, M., Endo, M., Ohashi, T., and Eto, Y. (2014) A practical fluorometric assay method to measure lysosomal acid lipase activity in dried blood spots for the screening of cholesteryl ester storage disease and Wolman disease. *Mol. Genet. Metab.* **111**, 193–196
88. Grisham, M. B., Johnson, G. G., and Lancaster, J. R., Jr. (1996) Quantitation of nitrate and nitrite in extracellular fluids. *Met. Enzymol.* **268**, 237–246
89. Bryan, N. S., and Grisham, M. B. (2007) Methods to detect nitric oxide and its metabolites in biological samples. *Free Radic. Biol. Med.* **43**, 645–657
90. Spath, G. F., and Beverley, S. M. (2001) A lipophosphoglycan-independent method for isolation of infective Leishmania metacyclic promastigotes by density gradient centrifugation. *Exp. Parasitol.* **99**, 97–103